Article:
Karageorghis, A, Lesnic, D and Marin, L (2014) The method of fundamental solutions for an inverse boundary value problem in static thermo-elasticity. Computers and Structures, 135. 32 - 39. ISSN: 0045-7949

https://doi.org/10.1016/j.compstruc.2014.01.007

The method of fundamental solutions for an inverse boundary value problem in static thermo-elasticity

A. Karageorghis[1,*], D. Lesnic[2,†], and L. Marin[3,4,‡]

[1]Department of Mathematics and Statistics, University of Cyprus/Πανεπιστήμιο Κύπρου,

P.O.Box 20537, 1678 Nicosia/Λευκωσία, Cyprus/Κύπρος

[2]Department of Applied Mathematics, University of Leeds, Leeds LS2 9JT, UK

[3]Department of Mathematics, Faculty of Mathematics and Computer Science,

University of Bucharest, 14 Academiei, 010014 Bucharest, Romania

[4]Institute of Solid Mechanics, Romanian Academy, 15 Constantin Mille, 010141 Bucharest, Romania

Abstract

The inverse problem of coupled static thermo-elasticity in which one has to determine the thermo-elastic stress state in a body from displacements and temperature given on a subset of the boundary is considered. A regularized method of fundamental solutions is employed in order to find a stable numerical solution to this ill-posed, but linear coupled inverse problem. The choice of the regularization parameter is based on the L-curve criterion. Numerical results are presented and discussed.

2000 Mathematics Subject Classification. Primary 33A65, 65N35; Secondary 65N22, 65F05, 35J05.

Keywords: thermo-elasticity; method of fundamental solutions; inverse problem.

1 Introduction

Whenever a solid is subject to heating conditions that give rise to a temperature distribution which produces thermal expansions throughout its volume, the structure is subject to thermo-elastic loadings. In much experimental research concerning the determination of thermo-elastic fields in a nuclear reactor or in structures of

*Corresponding author. E-mail: andreask@ucy.ac.cy

†E-mail: amt5ld@maths.leeds.ac.uk

‡E-mail: marin.liviu@gmail.com,liviu.marin@fmi.unibuc.ro

spacecraft and propulsion systems, measurements are possible on only an accessible part of the surface of the body. The remaining surface is usually in contact with a hostile environment and it is therefore very difficult or even impossible to place thermo-couples, heat flux probes, or strain gauges on it. In such a situation, one has to find the thermo-elastic stress state in the body by using displacements and temperature measurements taken on a subset of the boundary. In this study, this inverse problem of coupled thermo-elasticity in the static regime is solved numerically, apparently, for the first time. For related Cauchy inverse boundary condition numerical reconstructions in static thermo-elasticity the reader is referred to [3–5].

Since the problem is linear and we assume that the thermal and mechanical properties of the material are constant, the numerical technique we choose to employ to solve this problem is the method of fundamental solutions (MFS) which offers several advantages over the more established boundary element method (BEM) [24]. In particular, as stated in [11], the MFS is meshless in the sense that only a collection of points is required for the discretization of the problem under investigation. Unlike the BEM, no potentially troublesome integration is required in the MFS. These features make the MFS very easy to implement, in particular for problems in complex geometries and three dimensions. Moreover, unlike domain discretization methods such as the finite element (FEM) or finite difference (FDM) methods, it is a boundary method which means that only the boundary of the solution domain needs to be considered. This makes it particularly attractive for the solution of boundary value problems in which the boundary is of prime interest, such as inverse problems and free boundary problems. Finally, like the BEM it can easily deal with infinite domains by incorporating the behaviour of the solution of the problem at infinity into the fundamental solution of the governing equation. Because of its advantages, the MFS has been used extensively over the last decade for the solution of inverse problems [11]. In the particular problem under investigation because of the way the particular solution is derived it appears natural to use the MFS. The disadvantage of the MFS is that, like the BEM, it cannot be readily applied to problems in which the fundamental solution of the operator in the governing equation is not known explicitly or to inhomogeneous equations. In addition, a disadvantage of the MFS over the BEM is that the optimal location of the pseudo-boundary on which the singularities are to be placed is, in general, not known. We finally mention that a few different meshless boundary discretization techniques, different than, but related to the MFS have recently been introduced by W. Chen and his co-workers, see e.g. [6, 7].

The mathematical formulation of the problem is given in Section 2. In Section 3 we describe the MFS for the

solution of the problem in question. Furthermore, the Tikhonov regularization method with the choice of the regularization parameter given by the L-curve criterion is employed in order to obtain a stable solution. This stability is investigated in Section 4 with respect to noise in the input data. Finally, the conclusions drawn from this work are presented in Section 5.

2 Mathematical formulation

Consider a linear-elastic homogeneous, mechanically and thermally isotropic body occupying a simply connected domain Ω bounded by a smooth boundary $\partial\Omega$. The body is subjected to an unknown temperature field with sources outside Ω and we assume that other internal heat sources or body forces are absent. We consider practical applications involving high temperatures or hostile environments in which a part of the boundary $\Gamma_2 \subset \partial\Omega$ is inaccessible to measurements. In this case measurements of the displacements and temperature are available on the remaining accessible part $\Gamma_1 = \partial\Omega \backslash \Gamma_2$. Then the inverse problem of coupled static thermo-elasticity requires finding the displacement $\boldsymbol{u}$ and the temperature T satisfying the Navier-Lamé system [16, 20]

$$\mathcal{L}\boldsymbol{u} + \overline{\gamma}\nabla T = 0, \qquad \text{in} \qquad \Omega, \tag{1}$$

and the steady-state heat conduction Laplace equation

$$\kappa\, \Delta T = 0, \qquad \text{in} \qquad \Omega, \tag{2}$$

where $\kappa > 0$ is the thermal conductivity, $\overline{\gamma} = \dfrac{2G\overline{\alpha}_{\mathrm{T}}(1+\overline{\nu})}{1-2\overline{\nu}}$, G is the shear modulus,

$$\overline{\nu} = \begin{cases} \nu & \text{plane strain} \\ \nu/(1+\nu) & \text{plane stress} \end{cases} \quad \text{and} \quad \overline{\alpha}_{\mathrm{T}} = \begin{cases} \alpha_{\mathrm{T}} & \text{plane strain} \\ \alpha_{\mathrm{T}}(1+\nu)/(1+2\nu) & \text{plane stress,} \end{cases} \tag{3}$$

where α_{T} is the coefficient of thermal expansion, ν is the Poisson ratio and

$$\mathcal{L}\boldsymbol{u} = -G\left[\nabla\cdot\left(\nabla\boldsymbol{u} + (\nabla\boldsymbol{u})^{\mathsf{T}}\right) + \frac{2\overline{\nu}}{1-2\overline{\nu}}\nabla\left(\nabla\cdot\boldsymbol{u}\right)\right]. \tag{4}$$

In (4) and in the sequel the superscript T denotes the transpose of the matrix $\nabla\boldsymbol{u}$. The governing equations (1) and (2) have to be solved subject to the coupled boundary conditions

$$\boldsymbol{\sigma}(\boldsymbol{u})\boldsymbol{n} - \overline{\gamma}\, T\, \boldsymbol{n} = \boldsymbol{f}, \qquad \text{on} \qquad \partial\Omega, \tag{5}$$

where $\boldsymbol{n}$ is the outward unit normal to $\partial\Omega$ and the stress tensor is

$$\boldsymbol{\sigma}(\boldsymbol{u}) = 2G\left[\boldsymbol{\varepsilon} + \frac{\overline{\nu}}{1-2\overline{\nu}}\mathrm{tr}(\boldsymbol{\varepsilon})I\right], \tag{6}$$

and

$$\boldsymbol{\varepsilon}(\boldsymbol{u}) = \frac{1}{2}\left(\nabla\boldsymbol{u} + (\nabla\boldsymbol{u})^{\mathsf{T}}\right) \tag{7}$$

is the strain tensor. In (6), $\mathrm{tr}(\boldsymbol{\varepsilon})$ denotes the trace of the strain tensor. The left-hand side of equation (5) represents the traction vector $\boldsymbol{t}$, whilst its right-hand side $\boldsymbol{f}$ is a known vector function.

If T is prescribed on the whole boundary $\partial\Omega$ then, this gives rise to the direct problem in thermo-elasticity which is well-posed up to a rigid body displacement. However, in our inverse problem only the part Γ_1 of the boundary $\partial\Omega$ is accessible to measurement and on it we prescribe both the temperature and the displacement, namely,

$$T = \tilde{T}, \qquad \text{on} \qquad \Gamma_1, \tag{8a}$$

$$\boldsymbol{u} = \tilde{\boldsymbol{u}}, \qquad \text{on} \qquad \Gamma_1. \tag{8b}$$

The uniqueness of solution of the inverse problem (1)-(2), (5) and (8) was proved in [13, 14]. However, the problem is still ill-posed since small errors in the input data (8a) and (8b) cause large errors in the output solution $(\boldsymbol{u}, T)$ in Ω and, especially in the heat flux

$$q := -\kappa\nabla T\cdot\boldsymbol{n} \qquad \text{on} \qquad \Gamma_2, \tag{9a}$$

and traction

$$\boldsymbol{t} := \boldsymbol{\sigma}(\boldsymbol{u})\boldsymbol{n} - \overline{\gamma}\,T\,\boldsymbol{n}, \qquad \text{on} \qquad \Gamma_2. \tag{9b}$$

It is worth mentioning, that a related but decoupled Cauchy inverse and ill-posed problem consisting of equations (1)-(2) with (8a)-(8b) and

$$-\kappa\nabla T\cdot\boldsymbol{n} = \tilde{q} \qquad \text{on} \qquad \Gamma_1, \tag{10a}$$

$$\boldsymbol{\sigma}(\boldsymbol{u})\boldsymbol{n} - \overline{\gamma}\,T\,\boldsymbol{n} = \tilde{\boldsymbol{t}}, \qquad \text{on} \qquad \Gamma_1, \tag{10b}$$

see [3], has recently been solved using the MFS combined with the Tikhonov regularization in [18]. We also remark that from (5) and (8a) we obtain

$$\boldsymbol{\sigma}(\boldsymbol{u})\boldsymbol{n} = \boldsymbol{f} + \overline{\gamma}\,\tilde{T}\,\boldsymbol{n}, \qquad \text{on} \qquad \Gamma_1, \tag{11}$$

which together with (8b) form a set of Cauchy data prescribed on Γ_1.

3 The method of fundamental solutions (MFS)

The combination of the MFS with the method of particular solutions (MPS) for approximating a pair solution $(\boldsymbol{u}, T)$ of (1) and (2) is described in [17] and [12], in two and three dimensions, respectively.

In this section, we shall consider the two-dimensional case and describe the regularized MFS for solving the inverse problem (1)-(2), (5) and (8).

First, in the MFS for the Laplace equation (2) we seek the approximation of the temperature as

$$T_N(\boldsymbol{x}) = \sum_{\ell=1}^{N} c_\ell F(\boldsymbol{x}, \boldsymbol{\xi}_\ell), \qquad \boldsymbol{x} \in \overline{\Omega} \tag{12}$$

where the sources $\boldsymbol{\xi}_\ell \notin \overline{\Omega}$ and

$$F(\boldsymbol{x}, \boldsymbol{\xi}_\ell) = -\frac{1}{2\pi\kappa} \log|\boldsymbol{x} - \boldsymbol{\xi}_\ell| \tag{13}$$

is the fundamental solution of the two-dimensional Laplace equation (2).

Introducing (12) into (1) yields

$$\mathcal{L}\boldsymbol{u}(\boldsymbol{x}) = \frac{\overline{\gamma}}{2\pi\kappa} \sum_{\ell=1}^{N} c_\ell \frac{(x_1 - \xi_{1,\ell}, x_2 - \xi_{2,\ell})}{|\boldsymbol{x} - \boldsymbol{\xi}_\ell|^2}, \qquad \boldsymbol{x} = (x_1, x_2) \in \Omega, \tag{14}$$

where $\boldsymbol{\xi}_\ell = (\xi_{1,\ell}, \xi_{2,\ell})$ for $\ell = \overline{1, N}$. Then, using the MPS one seeks, see [17],

$$\boldsymbol{u} = \boldsymbol{u}_H + \boldsymbol{u}_P, \tag{15}$$

where

$$\mathcal{L}\boldsymbol{u}_H = \boldsymbol{0} \quad \text{in} \quad \Omega, \tag{16}$$

and

$$\boldsymbol{u}_P(\boldsymbol{x}) = -\frac{\overline{\alpha}_{\mathrm{T}}}{4\pi\kappa} \left(\frac{1+\overline{\nu}}{1-\overline{\nu}}\right) \sum_{\ell=1}^{N} c_\ell (\boldsymbol{x} - \boldsymbol{\xi}_\ell) \log|\boldsymbol{x} - \boldsymbol{\xi}_\ell|, \qquad \boldsymbol{x} \in \Omega \tag{17}$$

is a particular solution of (14).

We further apply the MFS to the Lamé homogeneous system (16) to approximate, see [15],

$$\boldsymbol{u}_H(\boldsymbol{x}) = \sum_{\ell=1}^{N} U(\boldsymbol{x}, \boldsymbol{\xi}_\ell)\boldsymbol{d}_\ell, \qquad \boldsymbol{x} \in \overline{\Omega}, \tag{18}$$

where $\boldsymbol{d}_\ell = (d_{1_\ell}, d_{2_\ell})$ and

$$U_{ij}(\boldsymbol{x}, \boldsymbol{\xi}) = \frac{1}{8\pi G(1-\overline{\nu})}\left[-(3-4\overline{\nu})\log|\boldsymbol{x}-\boldsymbol{\xi}|\,\delta_{ij} + \frac{(x_i-\xi_i)(x_j-\xi_j)}{|\boldsymbol{x}-\boldsymbol{\xi}|^2}\right], \quad i,j=1,2 \tag{19}$$

is the fundamental solution matrix of the Lamé homogeneous system (16) and δ_{ij} is the Kronecker delta tensor. The approximations (18) and (12) of the solution $(\boldsymbol{u}, T)$, via (17), contain $3N$ unknown real coefficients $(c_\ell)_{\ell=\overline{1,N}}$ and $(\boldsymbol{d}_\ell)_{\ell=\overline{1,N}} = (d_{1_\ell}, d_{2_\ell})_{\ell=\overline{1,N}}$. In order to determine these coefficients we impose the boundary conditions (5), (8a) and (8b). As boundary collocation points we take the points $(\boldsymbol{x}_j)_{j=\overline{1,N}}$ of which the first $(\boldsymbol{x}_j)_{j=\overline{1,N_1}}$ are uniformly distributed on Γ_1 and the remaining $(\boldsymbol{x}_j)_{j=\overline{N_1+1,N}}$ are uniformly distributed on Γ_2. Collocating (8a) and (8b) at $(\boldsymbol{x}_j)_{j=\overline{1,N_1}}$ yields $3N_1$ equations given by

$$\sum_{\ell=1}^{N} c_\ell F(\boldsymbol{x}_m, \boldsymbol{\xi}_\ell) = \tilde{T}(\boldsymbol{x}_m), \quad m = \overline{1, N_1} \tag{20a}$$

and

$$\sum_{\ell=1}^{N} U(\boldsymbol{x}_m, \boldsymbol{\xi}_\ell)\boldsymbol{d}_\ell + \frac{\overline{\alpha}_{\mathrm{T}}}{2}\left(\frac{1+\overline{\nu}}{1-\overline{\nu}}\right)\sum_{\ell=1}^{N} c_\ell(\boldsymbol{x}_m - \boldsymbol{\xi}_\ell)F(\boldsymbol{x}_m, \boldsymbol{\xi}_\ell) = \tilde{\boldsymbol{u}}(\boldsymbol{x}_m), \quad m = \overline{1, N_1}. \tag{20b}$$

In order to impose (5) we need to first calculate the stress tensors $\boldsymbol{\sigma}(\boldsymbol{u}_P)$ and $\boldsymbol{\sigma}(\boldsymbol{u}_H)$ from (17) and (18), respectively. First, as a direct consequence of (17) we have that the particular traction is given by, [17],

$$\boldsymbol{t}_P(\boldsymbol{x}) = -\frac{G\overline{\alpha}_{\mathrm{T}}}{2\pi\kappa}\left(\frac{1+\overline{\nu}}{1-\overline{\nu}}\right)\sum_{\ell=1}^{N} c_\ell\left[\frac{1}{1-2\overline{\nu}}\left(\log|\boldsymbol{x}-\boldsymbol{\xi}_\ell| + \overline{\nu}\right)\boldsymbol{n}(\boldsymbol{x}) + \frac{(\boldsymbol{x}-\boldsymbol{\xi}_\ell)\cdot\boldsymbol{n}(\boldsymbol{x})}{|\boldsymbol{x}-\boldsymbol{\xi}_\ell|^2}(\boldsymbol{x}-\boldsymbol{\xi}_\ell)\right], \qquad \boldsymbol{x} \in \partial\Omega. \tag{21}$$

Secondly, from (18) we obtain that the homogeneous traction vector is given by, [17],

$$\boldsymbol{t}_H(\boldsymbol{x}) = \sum_{\ell=1}^{N} \mathrm{T}(\boldsymbol{x}, \boldsymbol{\xi}_\ell)\boldsymbol{d}_\ell, \qquad \boldsymbol{x} \in \partial\Omega, \tag{22}$$

where T is the fundamental solution for the traction vector given by, see [1],

$$\begin{aligned}\mathrm{T}_{1j}(\boldsymbol{x}, \boldsymbol{\xi}) = {} & \frac{2G}{1-2\overline{\nu}}\left[(1-\overline{\nu})\frac{\partial U_{1j}}{\partial x_1}(\boldsymbol{x}, \boldsymbol{\xi}) + \overline{\nu}\frac{\partial U_{2j}}{\partial x_2}(\boldsymbol{x}, \boldsymbol{\xi})\right] n_1(\boldsymbol{x}) \\ & + G\left[\frac{\partial U_{1j}}{\partial x_2}(\boldsymbol{x}, \boldsymbol{\xi}) + \frac{\partial U_{2j}}{\partial x_1}(\boldsymbol{x}, \boldsymbol{\xi})\right] n_2(\boldsymbol{x}), \quad j = 1, 2,\end{aligned} \tag{23a}$$

$$\begin{aligned}\mathrm{T}_{2j}(\boldsymbol{x}, \boldsymbol{\xi}) = {} & G\left[\frac{\partial U_{1j}}{\partial x_2}(\boldsymbol{x}, \boldsymbol{\xi}) + \frac{\partial U_{2j}}{\partial x_1}(\boldsymbol{x}, \boldsymbol{\xi})\right] n_1(\boldsymbol{x}) \\ & + \frac{2G}{1-2\overline{\nu}}\left[\overline{\nu}\frac{\partial U_{1j}}{\partial x_1}(\boldsymbol{x}, \boldsymbol{\xi}) + (1-\overline{\nu})\frac{\partial U_{2j}}{\partial x_2}(\boldsymbol{x}, \boldsymbol{\xi})\right] n_2(\boldsymbol{x}), \quad j = 1, 2.\end{aligned} \tag{23b}$$

Rearranging we obtain that (5) is given by

$$\boldsymbol{t} = \boldsymbol{t}_P + \boldsymbol{t}_H = \boldsymbol{f}, \tag{24}$$

or

$$\sum_{\ell=1}^{N} \mathrm{T}(\boldsymbol{x}_m, \boldsymbol{\xi}_\ell)\boldsymbol{d}_\ell - \frac{G\overline{\alpha}_{\mathrm{T}}}{2\pi\kappa}\left(\frac{1+\overline{\nu}}{1-\overline{\nu}}\right)\sum_{\ell=1}^{N} c_\ell \left[\left(-\log|\boldsymbol{x}_m - \boldsymbol{\xi}_\ell| + \frac{\overline{\nu}}{1-2\overline{\nu}}\right)\boldsymbol{n}(\boldsymbol{x}_m) + \frac{(\boldsymbol{x}_m - \boldsymbol{\xi}_\ell)\cdot\boldsymbol{n}(\boldsymbol{x}_m)}{|\boldsymbol{x}_m - \boldsymbol{\xi}_\ell|^2}(\boldsymbol{x}_m - \boldsymbol{\xi}_\ell)\right] = \boldsymbol{f}(\boldsymbol{x}_m), \quad m = \overline{1, N}. \tag{25}$$

In summary, equations (20a), (20b) and (25) form a system of $3N_1 + 2N$ linear equations in $3N$ unknowns. We require that $3N_1 \geq N$ and solve this system using the Tikhonov regularization of order zero with the choice of the regularization parameter given by the L-curve method. This rather standard technique has been used in many studies dealing with linear ill-posed problems, see for more details [10].

The particular solution for the displacements in the proposed approach is expressed using the MFS which appears very natural in this context. In order to obtain a particular solution for the displacements in the case when instead of equation (2) we have its inhomogeneous version, namely the Poisson equation $\Delta T = Q$, where Q is a given heat source, or the heterogeneous conductivity equation $\nabla \cdot (\kappa(\boldsymbol{x})\nabla T) = 0$, one would have to use a more general purpose method such asthe multiple reciprocity [21] or the dual reciprocity BEMs [22].

4 Numerical examples

Throughout this section the material constants were taken to be as follows: $G = 4.8 \times 10^{10}\mathrm{N/m}^2$, $\nu = 0.34$, $\kappa = 4.01\mathrm{Wm}^{-1}\mathrm{K}^{-1}$ and $\alpha_{\mathrm{T}} = 16.5 \times 10^{-6}\ {}^{\circ}\mathrm{C}^{-1}$. The L-curves and the Tikhonov regularization were carried out using the routine `tikhonov` from Hansen's regularization tools package [8, 9]. In the first three examples we assume that the material is in the plane strain state, while in the fourth example we assume that the material is in the plane stress state. In order to study the stability of the proposed approach noise was added to the right hand sides $\tilde{T}(\boldsymbol{x}_m)$ and $\tilde{\boldsymbol{u}}(\boldsymbol{x}_m),\ m = \overline{1, N_1}$ of (20a) and (20b), respectively. In particular, instead of considering $\tilde{T}(\boldsymbol{x}_m)$ and $\tilde{\boldsymbol{u}}(\boldsymbol{x}_m),\ m = \overline{1, N_1}$, we considered $(1 + p\varrho_m)\tilde{T}(\boldsymbol{x}_m)$ and $(1 + p\varrho_m)\tilde{\boldsymbol{u}}(\boldsymbol{x}_m),\ m = \overline{1, N_1}$, respectively, where p is the percentage noise added and $\boldsymbol{\varrho} = [\varrho_1, \ldots, \varrho_{N_1}]$ is a random noisy variable vector in [-1, 1] generated using the `MATLAB` command `-1+2*rand(1,`N_1`)`.

4.1 Example 1

We first consider an example in the unit disk with exact solution

$$T(\boldsymbol{x}) = 100 \log |\boldsymbol{x} - \boldsymbol{x}_0|, \quad \boldsymbol{u}(\boldsymbol{x}) = \frac{\overline{\alpha}_{\mathrm{T}}}{2} \left(\frac{1+\overline{\nu}}{1-\overline{\nu}} \right) T(\boldsymbol{x})(\boldsymbol{x} - \boldsymbol{x}_0), \quad \text{where} \quad \boldsymbol{x}_0 = (8, 1). \tag{26}$$

The boundary Γ_1 is taken to be the upper half of the circular boundary $\partial\Omega$, i.e. $\Gamma_1 = \{(\cos\vartheta, \sin\vartheta), 0 \leq \vartheta \leq \pi\}$. The radius of the outer circle on which the sources are placed is taken to be 4. We also take $N_1 = 60$ and $N = 120$. In Figures 1 and 2 we present the results for the temperature T, the flux q and the displacement vector $\boldsymbol{u}$ obtained on the boundary $\Gamma_2 = \partial\Omega \backslash \Gamma_1$ for noise $p = 0$ and 1%, respectively. There is no need to present the traction $\boldsymbol{t}$ on Γ_2 since it is given in terms of $T|_{\Gamma_2}$ from equations (5) and (9b). The solution was calculated at 101 uniformly distributed points on the boundary Γ_2 (different than the collocation points). First, the results presented in Figure 1 show that for exact data, i.e. $p = 0$, and no regularization imposed there is excellent agreement between the exact and MFS approximations for all illustrated quantities. In fact, the curves in Figure 1 are indistinguishable. However, this unregularized solution is not very useful in practice since any small error in the input data will cause a large (unbounded and highly oscillatory) error in the output solution, as illustrated in Figure 2. Consequently, regularization is necessary and, as mentioned at the end of Section 3, in this study we employ the Tikhonov regularization method with the choice of the regularization parameter $\lambda > 0$ given by the corner of the L-curve, [10]. In Figure 3 we present the L-curves obtained for noise $p = 1\%, 3\%$ and 5%. This figure clearly indicates the presence of a sharp corner of the L-curve which corresponds to the values of $\lambda_{\mathrm{opt}} \in \left\{10^{-2}, 10^{-1}, 10^{-1}\right\}$ for $p \in \{1, 3, 5\}\,\%$, respectively. In Figures 4(a)-4(d) we present the results for the temperature T, the flux q and the displacement vector $\boldsymbol{u}$ obtained on Γ_2 for noise $p = 1\%$, with the regularization parameter $\lambda = 10^{-7} < \lambda_{\mathrm{opt}}, \lambda = 10^{-2} = \lambda_{\mathrm{opt}}, \lambda = 10 > \lambda_{\mathrm{opt}}$, respectively. From these figures it can be seen that if λ is too small, i.e. $\lambda = 10^{-7} \ll \lambda_{\mathrm{opt}} = 10^{-2}$, the solutions are not sufficiently regularized and are still unstable. If λ is too large, i.e. $\lambda_{\mathrm{opt}} = 10^{-2} \ll \lambda = 10^{1}$, the numerical solutions are stable but largely different from the exact solutions. As is often the case with inverse and ill-posed problems, in order to balance between the two extremes one needs to compromise and choose an appropriate λ_{opt} which is neither too small nor too large. Such a parameter is $\lambda_{\mathrm{opt}} = 10^{-2}$, as given by the L-curve of Figure 3 for $p = 1\%$ noise. With this choice, the numerical results presented in the middle sub-figures of Figures 4(a)-4(d) show that a stable and accurate solution can be obtained. Furthermore, by comparing Figure 4(a) with Figures 4(c), 4(d) it can be seen that the ill-posedness manifests itself more strongly in the boundary temperature than in the displacement. The

λ	10^{-7}	10^{-2}	10
T	3.403(+1)	1.207(-2)	8.318(-1)
q	8.593(+2)	1.859(-1)	9.983(-1)
u_1	1.887	1.466(-3)	9.420(-1)
u_2	1.399(+1)	6.202(-3)	9.090(-1)

Table 1: Example 1: Maximum relative errors for T, q and $\boldsymbol{u}$ on Γ_2 for noise $p = 1\%$ and $\lambda = 10^{-7}, 10^{-2}$ and 10.

corresponding maximum relative errors on the boundary Γ_2 for T, q and $\boldsymbol{u}$ for noise $p = 1\%$ and $\lambda = 10^{-7}, 10^{-2}$ and 10 are presented in Table 1.

Example 1 presented the determined situation in which the length of the over-prescribed boundary Γ_1 is equal to the length of the under-prescribed boundary Γ_2. The next two Examples 2 and 3 consider the under-determined and over-determined cases, respectively.

4.2 Example 2

In this example, we consider the exact solution given by (26), but now with the boundary Γ_1 taken to be the first third of the circular boundary $\partial\Omega$, i.e. $\Gamma_1 = \{(\cos\vartheta, \sin\vartheta), 0 \leq \vartheta \leq 2\pi/3\}$. The radius of the outer circle on which the sources are placed is, as in the previous example, taken to be 4, and we also take $N_1 = 40, N = 120$. In Figure 5 we present the L-curves obtained for noise $p = 1\%, 3\%$ and 5%. The corners of the L-curves correspond to the values of $\lambda_{\text{opt}} \in \left\{10^{-2}, 10^{-2}, 10^{-1}\right\}$ for $p \in \{1, 3, 5\}\,\%$, respectively. In Figures 6(a)-6(d) we present the results for the temperature T, the flux q and the displacement vector $\boldsymbol{u}$ obtained on the boundary $\Gamma_2 = \partial\Omega\backslash\Gamma_1$, for noise $p = 3\%$, with $\lambda = 10^{-7} < \lambda_{\text{opt}}, \lambda = 10^{-2} = \lambda_{\text{opt}}, \lambda = 10 > \lambda_{\text{opt}}$, respectively. The solution was calculated at 102 uniformly distributed points on Γ_2 (different than the collocation points). Although not illustrated, it is reported that, as expected, for the same amount of noise p, the determined case of Example 1 produces better results in terms of both accuracy and stability than the under-determined case of Example 2. One can also observe that the corners of the L-curves in Figure 3 for Example 1 are slightly sharper than those in Figure 5 for Example 2. However, the numerical results presented in Figures 6(a)-6(d) for $p = 3\%$ noise show that stable and reasonably accurate reconstructions are still achievable even in this under-determined situation. The rest of the conclusions are consistent with those for Figures 4(a)-4(d) of Example 1.

For completeness, we next consider an over-determined case.

4.3 Example 3

We consider the exact solution given by (26), but now with the boundary Γ_1 taken to be the first two thirds of the circular boundary $\partial\Omega$, i.e. $\Gamma_1 = \{(\cos\vartheta, \sin\vartheta), 0 \leq \vartheta \leq 4\pi/3\}$. As in the previous examples, the radius of the outer circle on which the sources are placed is taken to be 4 and we take $N_1 = 80$ and $N = 120$. In Figure 7 we present the L-curves obtained for noise $p = 1\%, 3\%$ and 5%. The corners of the L-curves correspond to the values of $\lambda_{\text{opt}} \in \left\{10^{-2}, 10^{-2}, 10^{-1}\right\}$ for $p \in \{1, 3, 5\}\,\%$, respectively. In Figures 8(a)-8(d) we present the results for the temperature T, the flux q and the displacement vector $\boldsymbol{u}$ obtained on the boundary $\Gamma_2 = \partial\Omega\backslash\Gamma_1$, for noise $p = 5\%$, with $\lambda = 10^{-7} < \lambda_{\text{opt}}, \lambda = 10^{-1} = \lambda_{\text{opt}}, \lambda = 10 > \lambda_{\text{opt}}$, respectively. The solution was calculated at 51 uniformly distributed points on Γ_2 (different than the collocation points). The numerical results illustrated in Figures 8(a)-8(d) are consistent with those of Figures 4(a)-4(d) for Example 1 and Figures 6(a)-6(d) for Example 2. We also report that for the same amount of noise p, the over-determined case of Example 3 produces slightly better results than the determined case of Example 1. Moreover, as may be seen from Figures 8(a)-8(d), the additional noise present in the over-determined situation of Example 3 does not affect the stability of the numerical results.

4.4 Example 4

We finally consider an example from [18] in an annular domain defined by

$$\Omega = \left\{\boldsymbol{x} \in \mathbb{R}^2 | R_{\text{int}} < |\boldsymbol{x}| < R_{\text{out}}\right\},\ \partial\Omega = \Gamma_1 \cup \Gamma_2 \text{ where } \Gamma_1 = \left\{\boldsymbol{x} \in \mathbb{R}^2 |\ |\boldsymbol{x}| = R_{\text{out}}\right\}, \Gamma_2 = \left\{\boldsymbol{x} \in \mathbb{R}^2 |\ |\boldsymbol{x}| = R_{\text{int}}\right\},$$

with $R_{\text{int}} = 1, R_{\text{out}} = 2$. We consider the plane stress state and the exact solution

$$T(\boldsymbol{x}) = T_{\text{out}} \frac{\log(|\boldsymbol{x}|/R_{\text{int}})}{\log(R_{\text{out}}/R_{\text{int}})} + T_{\text{int}} \frac{\log(R_{\text{out}}/|\boldsymbol{x}|)}{\log(R_{\text{out}}/R_{\text{int}})}, \quad \boldsymbol{x} \in \overline{\Omega}, \tag{27a}$$

$$q(\boldsymbol{x}) = -\kappa \frac{T_{\text{out}} - T_{\text{int}}}{\log(R_{\text{out}}/R_{\text{int}})} \frac{\boldsymbol{x} \cdot \boldsymbol{n}}{|\boldsymbol{x}|^2}, \quad \boldsymbol{x} \in \partial\Omega, \tag{27b}$$

$$\boldsymbol{u}(\boldsymbol{x}) = \left[\frac{\overline{\alpha}_{\text{T}}}{2} \frac{1+\overline{\nu}}{1-\overline{\nu}} \frac{T_{\text{out}} - T_{\text{int}}}{\log(R_{\text{out}}/R_{\text{int}})} \log|\boldsymbol{x}| + \frac{1}{2G}\left(\frac{1-\nu}{1+\nu} V - \frac{W}{|\boldsymbol{x}|^2}\right)\right] \boldsymbol{x}, \quad \boldsymbol{x} \in \overline{\Omega}, \tag{27c}$$

$$\boldsymbol{t}(\boldsymbol{x}) = -\overline{\gamma} T \boldsymbol{n}(\boldsymbol{x}) - \begin{cases} \sigma_{\text{out}} \boldsymbol{n}(\boldsymbol{x}), & \boldsymbol{x} \in \Gamma_1, \\ \sigma_{\text{int}} \boldsymbol{n}(\boldsymbol{x}), & \boldsymbol{x} \in \Gamma_2, \end{cases} \tag{27d}$$

where

$$V = -\frac{\sigma_{\text{out}}^{(\text{H})} R_{\text{out}}^2 - \sigma_{\text{int}}^{(\text{H})} R_{\text{int}}^2}{R_{\text{out}}^2 - R_{\text{int}}^2}, \quad W = \frac{\left(\sigma_{\text{out}}^{(\text{H})} - \sigma_{\text{int}}^{(\text{H})}\right) R_{\text{out}}^2 R_{\text{int}}^2}{R_{\text{out}}^2 - R_{\text{int}}^2}, \tag{27e}$$

$$\sigma_{\text{out}}^{(\text{H})} = \sigma_{\text{out}} - \overline{\gamma} T_{\text{out}} + G\overline{\alpha}_{\text{T}} \frac{1+\overline{\nu}}{1-2\overline{\nu}} \left(\frac{T_{\text{out}} - T_{\text{int}}}{\log(R_{\text{out}}/R_{\text{int}})} \right) \left(\frac{1}{1-\overline{\nu}} \log R_{\text{out}} + 1 \right), \tag{27f}$$

$$\sigma_{\text{int}}^{(\text{H})} = \sigma_{\text{int}} - \overline{\gamma} T_{\text{int}} + G\overline{\alpha}_{\text{T}} \frac{1+\overline{\nu}}{1-2\overline{\nu}} \left(\frac{T_{\text{out}} - T_{\text{int}}}{\log(R_{\text{out}}/R_{\text{int}})} \right) \left(\frac{1}{1-\overline{\nu}} \log R_{\text{int}} + 1 \right). \tag{27g}$$

From (27a) one may easily see that $T|_{\Gamma_1} = T_{\text{out}}$ and $T|_{\Gamma_2} = T_{\text{int}}$ and we take $T_{\text{out}} = 2,\ T_{\text{int}} = 1$. We also take $\sigma_{\text{out}} = 2,\ \sigma_{\text{int}} = 1$. It is worth pointing out that in this example the domain Ω is not simply-connected and therefore the theorem of uniqueness of the solution of the inverse problem which holds for simply-connected domains, [13, 14], and which is yet to be established for multiply connected domains, cannot be strictly invoked. The radii of the outer and inner circles on which the singularities are placed are taken to be 4 and 0.5, respectively, and we take $N_1 = 80$ and $N = 160$. In Figures 9 and 10 we present the results for the temperature T, the flux q and the displacement vector $\boldsymbol{u}$ obtained on the boundary $\Gamma_2 = \partial\Omega \backslash \Gamma_1$ for noise $p = 0$ and 5%, respectively. The solution was calculated at 101 uniformly distributed points on the boundary Γ_2 (different than the collocation points). From Figure 9 it can be seen that for exact input data (8a)-(8b) the unregularized MFS solution is in very good agreement with the exact solution on Γ_2. In contrast, Figure 10 shows that for noisily perturbed input data (8a)-(8b), the unregularized MFS solution on Γ_2 becomes highly unstable, especially in the temperature and heat flux. Regularization is therefore necessary in order to achieve a stable solution.

In Figure 11 we present the L-curves obtained for noise $p = 1\%, 3\%$ and 5%. The corners of the L-curves correspond to the values of $\lambda_{\text{opt}} \in \left\{10^{-2}, 10^{-2}, 10^{-1}\right\}$ for $p \in \{1, 3, 5\}$ %, respectively. In Figures 12(a)-12(d) we present the results for the temperature T, the flux q and the displacement vector $\boldsymbol{u}$ obtained on the boundary Γ_2, for noise $p = 5\%$, with $\lambda = 10^{-10} < \lambda_{\text{opt}}, \lambda = 10^{-2} = \lambda_{\text{opt}}, \lambda = 10 > \lambda_{\text{opt}}$, respectively. From these figures it can be seen that stable and accurate numerical solutions are obtained if λ is chosen in accordance to the L-curve criterion illustrated in Figure 11.

5 Conclusions

In this paper, the MFS in conjunction with the MPS developed in [17] for the direct problem has been applied to solve in a stable manner an inverse linear boundary value problem of static coupled thermo-elasticity [13, 14]. To the best of our knowledge, this problem has never been solved before numerically. From this application we can draw the following conclusions/observations:

(i) To treat the ill-posedness of the problem the MFS was used in conjunction with the Tikhonov regularization method, with the mention that the Tikhonov regularized/stabilised solution was obtained by inverting the corresponding normal equation.

(ii) The choice of the optimal regularization parameter was based on Hansen's L-curve criterion, in the sense that this curve parameter was taken to correspond to the corner of the L-curve (i.e. the point of maximum curvature).

(iii) Stable and accurate numerical results have been obtained for the inverse boundary value problem under investigation in both simply and doubly connected geometries, with either an under-, equally- or over-determined boundary Γ_2.

The numerical solution of the inverse problems of quasi-static and dynamic coupled thermo-elasticity [13] will be the subject of a future study. In addition, the application of the MFS to complicated two- and three-dimensional crack identification problems such as those reported in [2, 19] with the BEM, and transient thermoelastic crack problems, as reported in [23] using the dual BEM could be another subject of future research.

Acknowledgements

The authors would like to thank the University of Cyprus for supporting this research. L. Marin also acknowledges the financial support received from the Romanian National Authority for Scientific Research (CNCS–UEFISCDI), project number PN–II–ID–PCE–2011–3–0521.

References

[1] M. H. Aliabadi, *The Boundary Element Method. Applications in Solids and Structures*, John Wiley and Sons, London, 2002, Volume 2.

[2] M. H. Aliabadi and S. C. Mellings, *Boundary element formulations for sensitivity analysis and crack identification*, Boundary integral formulations for inverse analysis, Adv. Bound. Elem. Ser., Comput. Mech., Southampton, 1997, pp. 93–117.

[3] B. H. Dennis and G. S. Dulikravich, *Simultaneous determination of temperatures, heat fluxes, deformations on inaccessible boundaries*, J. Heat. Transfer **121** (1999), 537–545.

[4] B. H. Dennis, G. S. Dulikravich, and S. Yoshimura, *A finite element formulation for the determination of unknown boundary conditions for 3-D steady thermoelastic problems*, J. Heat. Transfer **126** (2004), 110–118.

[5] B. H. Dennis, W Jin, G. S. Dulikravich, and J. Jaric, *Application of the finite element method to inverse problems in solid mechanics*, Int. J. Structural Changes in Solids - Mechanics and Applications **3** (2011), 11–21.

[6] Y. Gu, W. Chen, and C.-Z. Zhang, *Singular boundary method for solving plane strain elastostatic problems*, Int. J. Solids Struct. **48** (2011), 2549–2556.

[7] Y. Gu, W. Chen, and X.-Q. He, *Singular boundary method for steady-state heat conduction in three dimensional general anisotropic media*, Int. J. Heat Mass Transfer **55** (2012) 4837–4848.

[8] P. C. Hansen, *Regularization tools: a Matlab package for analysis and solution of discrete ill-posed problems*, Numer. Algorithms **6** (1994), 1–35.

[9] P. C. Hansen, *Regularization tools version 4.0 for Matlab 7.3*, Numer. Algorithms **46** (2007), 189–194, available at `www.netlib.org/numeralgo`.

[10] P. C. Hansen, *Discrete Inverse Problems: Insight and Algorithms*, SIAM, Philadelphia, 2010.

[11] A. Karageorghis, D. Lesnic, and L. Marin, *A survey of applications of the MFS to inverse problems*, Inverse Probl. Sci. Eng. **19** (2011), 309–336.

[12] A Karageorghis and Y.-S Smyrlis, *Matrix decomposition MFS algorithms for elasticity and thermo-elasticity problems in axisymmetric domains*, J. Comput. Appl. Math. **206** (2007), 774–795.

[13] V. A. Kozlov, V. G. Maz'ya, and A. V. Fomin, *The inverse problem of coupled thermo-elasticity*, Inverse Problems **10** (1994), 153–160.

[14] V. A. Kozlov, V. G. Maz'ya, and A. V. Fomin, *Uniqueness of the solution to an inverse thermoelasticity problem*, Computational Mathematics and Mathematical Physics **49** (2009), 525–531.

[15] V. D. Kupradze, *Potential Methods in the Theory of Elasticity*, Israel Program for Scientific Translations, Jerusalem, 1965.

[16] L. D. Landau and E. M. Lifshits, *Theory of Elasticity*, Elsevier, Oxford, 1986.

[17] L. Marin and A. Karageorghis, *The MFS-MPS for two-dimensional steady-state thermoelasticity problems*, Eng. Anal. Bound. Elem. **37** (2013), 1004–1020.

[18] L. Marin and A. Karageorghis, *The MFS for the Cauchy problem in two-dimensional steady-state linear thermoelasticity*, Int. J. Solids Struct. **50** (2013), 3387–3398.

[19] S. C. Mellings and M. H. Aliabadi, *Three-dimensional flaw identification using inverse analysis*, Internat. J. Engrg. Sci. **34** (1996), 453–469.

[20] A. Nowacki, *Thermoelasticity*, Pergamon Press, Oxford, 1986.

[21] A. J. Nowak and A. Neves, *The Multiple Reciprocity Boundary Element Method*, Computational Mechanics Publications, Southampton, 1994.

[22] P. W. Partridge, C. A. Brebbia, and L. C. Wrobel, *The Dual Reciprocity Boundary Element Method*, Computational Mechanics Publications, Southampton, 1992.

[23] N. N. V. Prasad, M. H. Aliabadi, and D. P. Rooke, *The dual boundary element method for transient thermoelastic crack problems*, Int. J. Solids Struct. **33** (1996), 2695–2718.

[24] V. Sladek and J. Sladek, *Boundary integral equation in thermoelasticity. Part I: General analysis*, Appl. Math. Model. **7** (1983), 413–418.

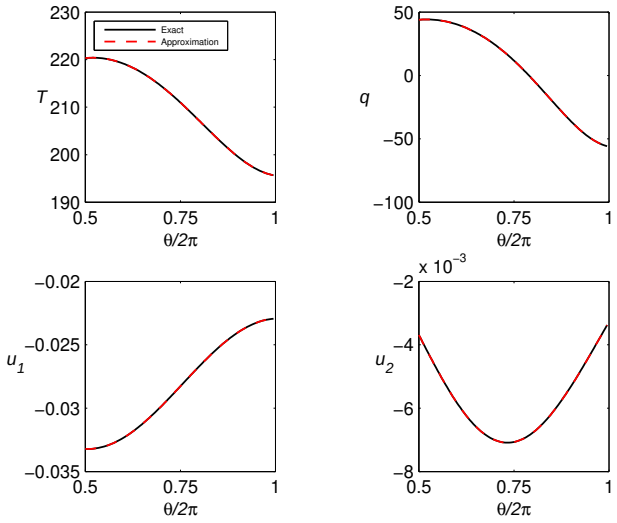

Figure 1: Example 1: Results on Γ_2 for no noise and no regularization.

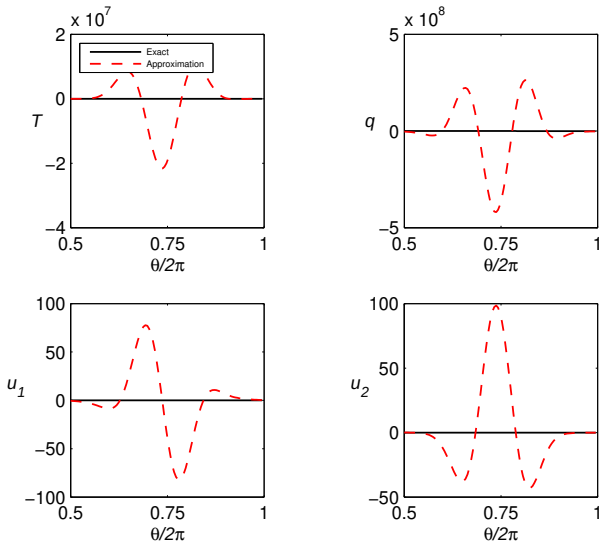

Figure 2: Example 1: Results on Γ_2 for noise $p = 1\%$ and no regularization.

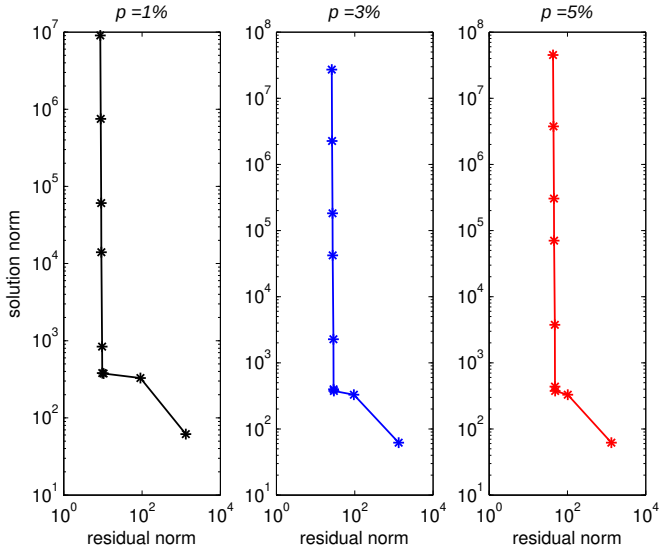

Figure 3: Example 1: L-curves for noise $p = 1\%, 3\%$ and 5%.

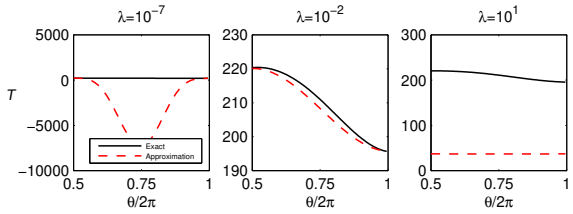

(a) $T|_{\Gamma_2}$

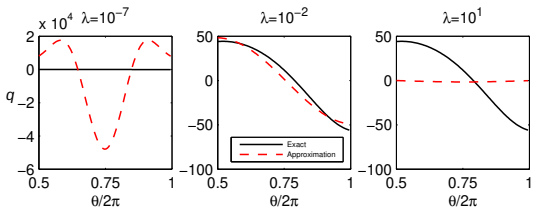

(b) $q|_{\Gamma_2}$

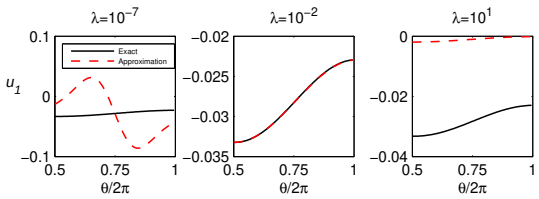

(c) $u_1|_{\Gamma_2}$

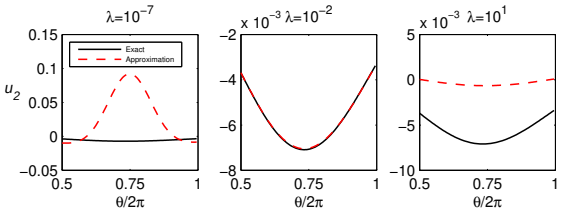

(d) $u_2|_{\Gamma_2}$

Figure 4: Example 1: Results for noise $p = 1\%$ with $\lambda < \lambda_{\text{opt}}, \lambda = \lambda_{\text{opt}}, \lambda > \lambda_{\text{opt}}$.

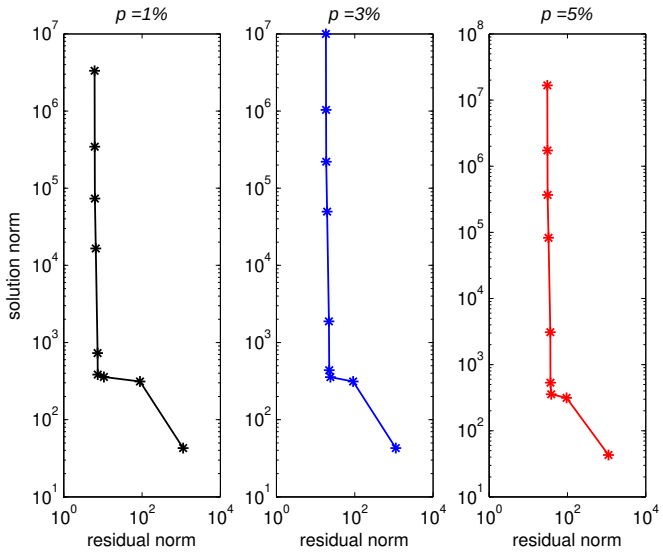

Figure 5: Example 2: L-curves for noise $p = 1\%, 3\%$ and 5%.

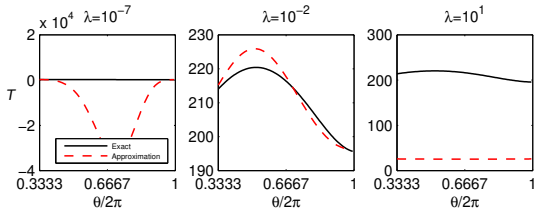

(a) $T|_{\Gamma_2}$

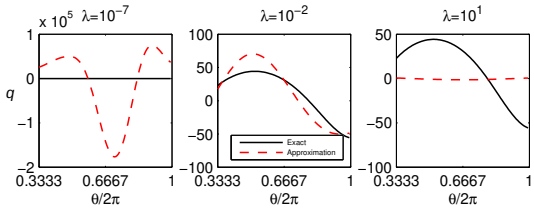

(b) $q|_{\Gamma_2}$

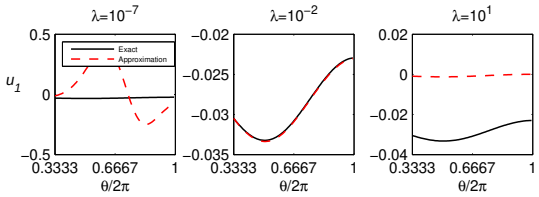

(c) $u_1|_{\Gamma_2}$

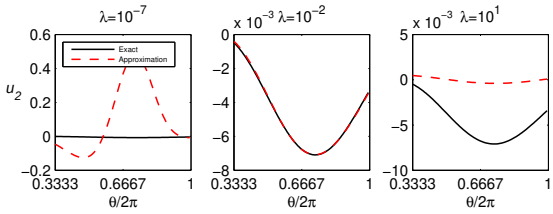

(d) $u_2|_{\Gamma_2}$

Figure 6: Example 2: Results for noise $p = 3\%$ with $\lambda < \lambda_{\text{opt}}, \lambda = \lambda_{\text{opt}}, \lambda > \lambda_{\text{opt}}$.

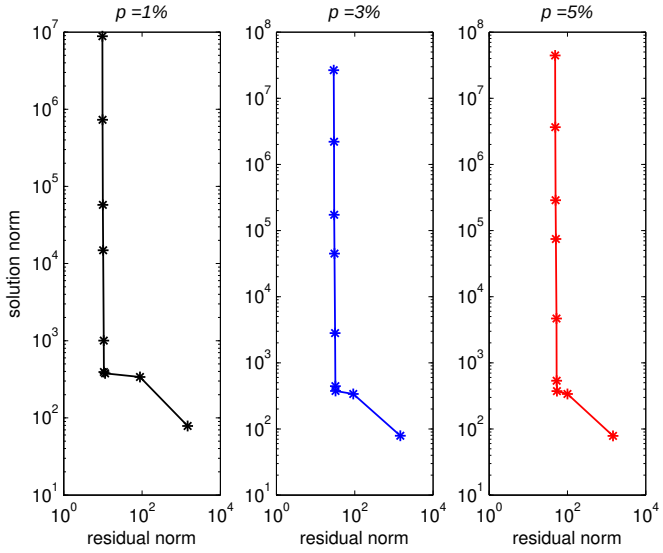

Figure 7: Example 3: L-curves for noise $p = 1\%, 3\%$ and 5%.

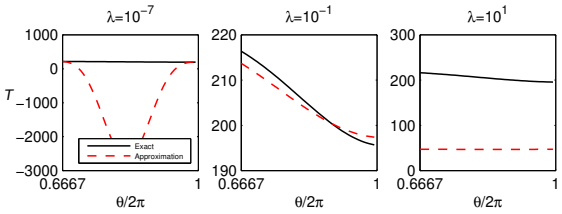

(a) $T|_{\Gamma_2}$

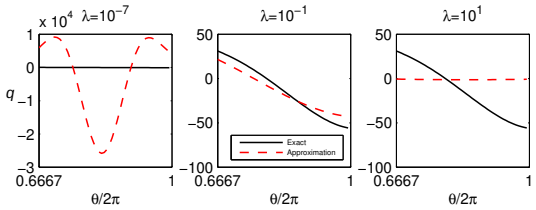

(b) $q|_{\Gamma_2}$

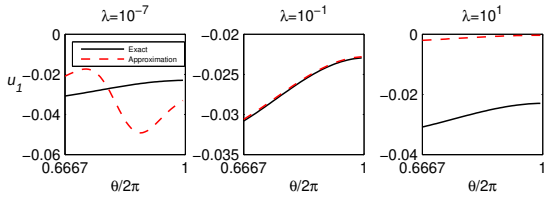

(c) $u_1|_{\Gamma_2}$

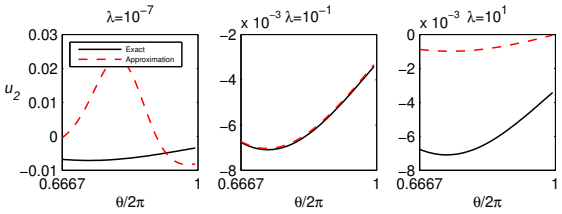

(d) $u_2|_{\Gamma_2}$

Figure 8: Example 3: Results for noise $p = 5\%$ with $\lambda < \lambda_{\text{opt}}, \lambda = \lambda_{\text{opt}}, \lambda > \lambda_{\text{opt}}$.

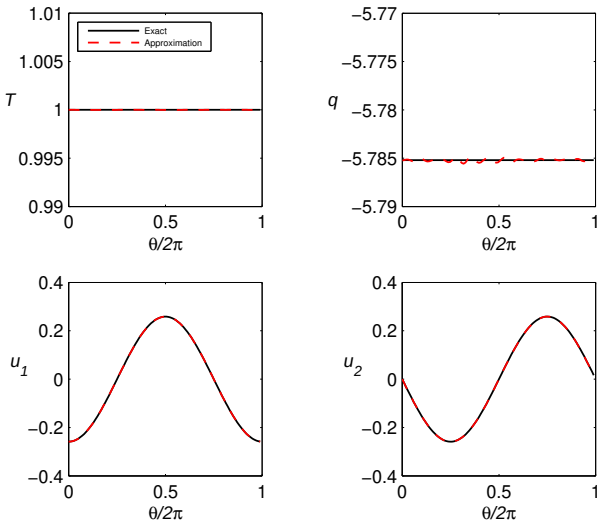

Figure 9: Example 4: Results on Γ_2 for no noise and no regularization.

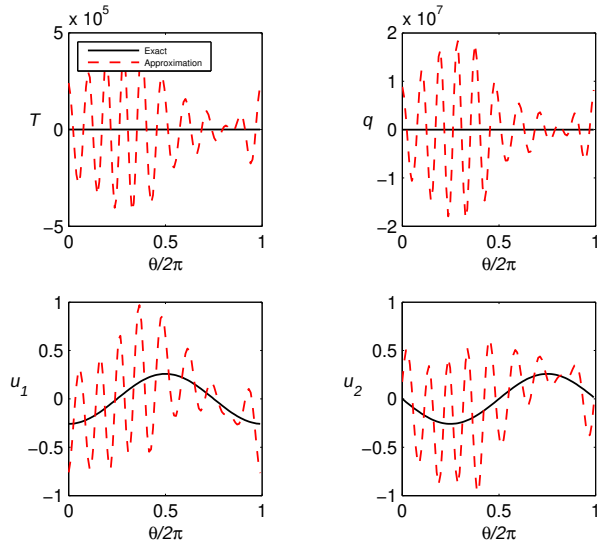

Figure 10: Example 4: Results on Γ_2 for noise $p = 5\%$ and no regularization.

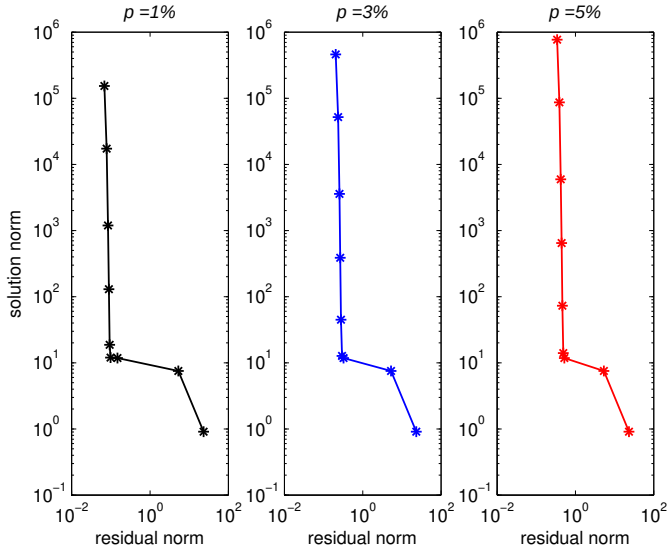

Figure 11: Example 4: L-curves for noise $p = 1\%, 3\%$ and 5%.

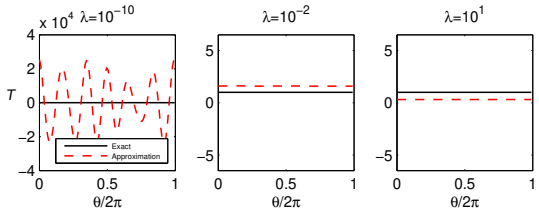

(a) $T|_{\Gamma_2}$

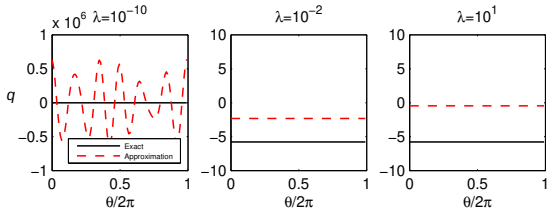

(b) $q|_{\Gamma_2}$

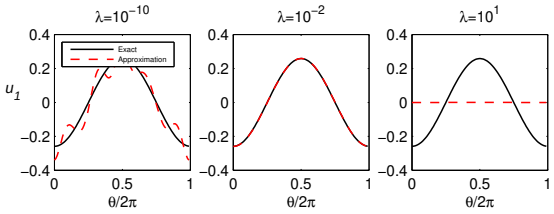

(c) $u_1|_{\Gamma_2}$

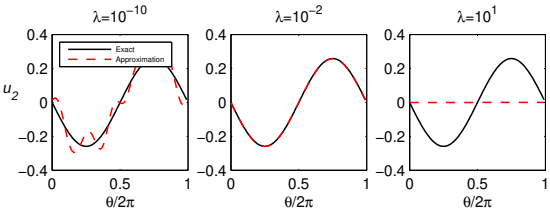

(d) $u_2|_{\Gamma_2}$

Figure 12: Example 4: Results for noise $p = 5\%$ with $\lambda < \lambda_{\text{opt}}, \lambda = \lambda_{\text{opt}}, \lambda > \lambda_{\text{opt}}$.